Experimental Investigation of Gypsum's Mechanical Properties Using Triaxial Compression Tests

by

Jiaxuan Shi

Department of Civil and Environmental Engineering
Duke University

Defense Date: March 27, 2025

Approved:

Manolis Veveakis, Co-chair

Henri Gavin, Co-chair

Laura Dalton

Thesis submitted in partial fulfillment of the requirements for the degree of Master of Science in the Department of Civil and Environmental Engineering in the Graduate School of Duke University
2025

ABSTRACT

Experimental Investigation of Gypsum's Mechanical Properties Using Triaxial Compression Tests

by

Jiaxuan Shi

Department of Civil and Environmental Engineering
Duke University

Defense Date: March 27, 2025

Approved:

Manolis Veveakis, Co-chair

Henri Gavin, Co-chair

Laura Dalton

An abstract of a thesis submitted in partial fulfillment of the requirements for the degree of Master of Science in the Department of Civil and Environmental Engineering in The Graduate School of Duke University
2025

Abstract

Gypsum is a widely used sulfate mineral, and it is an important construction material used to make plaster and drywall due to its rapid hardening and low thermal conductivity. However, its mechanical performance under varying stress conditions, particularly the influence of water content on strength and deformation behavior remains underexplored. This study investigates the mechanical properties of gypsum through triaxial testing, focusing on stress-strain response, failure modes, and the Mohr-Coulomb failure criterion. Wet gypsum specimens with pore saturations of 10%, 20%, and 40%, were subjected to controlled loading conditions (0.414 MPa) to evaluate the impact of moisture on mechanical strength. Experimental results demonstrate that increased water content reduces peak strength. X-ray micro-computed tomography (Micro-CT) was used to analyze internal microstructural changes, revealing variations in particle distribution, and observing cementations formed inside of the gypsum samples. This study offers better insights into the mechanical response of gypsum, supporting its effective application in geomechanics and engineering practices.

Dedication

I dedicate this thesis to my beloved family and Hope. They always stand by my side in every step of my life.

Contents

List of Figures

Acknowledgements

I would like to express my sincere gratitude to my advisor, Dr. Manolis Veveakis, for giving me the opportunity to explore the field of geomechanics. His guidance, expertise, and support have been invaluable throughout my research journey. I am especially grateful for the chance to engage in laboratory experiments, which have been a critical part of my learning and development.

I am also thankful to Professor Laura Dalton for her generous assistance with the CT scan analysis. Her expertise and willingness to help were instrumental in advancing my research and deepening my understanding of microstructural characterization.

A special thank you goes to Alexandre Sac-Morane, my PhD mentor, for his continuous support and guidance throughout this thesis. His insights, encouragement, and constructive feedback have been indispensable in navigating the challenges of this work.

Finally, I would like to acknowledge the support of my colleagues, and friends, whose encouragement have been a constant source of motivation throughout this journey.

1. Introduction

Gypsum is a widely occurring sulfate mineral extensively used in construction, particularly in the production of plaster and drywall, due to its low thermal conductivity and its ability to be shaped and hardened quickly (del Río-Merino et al., 2022). When mixed with water, gypsum undergoes hydration, forming a solid matrix that enhances its utility in interior applications. However, its inherent solubility in water renders it unsuitable for external construction, where prolonged exposure to moisture may lead to material degradation (Garg & Pundir, 2014). The physicochemical characteristics of gypsum, including particle size distribution and intrinsic dissolution rate, are critical factors influencing hydration reactions in binders containing Portland cement, particularly in the regulation of tricalcium aluminate interactions (Jin et al., 2020).

Geologically, gypsum is a sedimentary mineral commonly found in marine evaporite deposits and is among the first minerals to precipitate from seawater due to the relatively low solubility of calcium (Ca^{2+}) and sulfate (SO_4^{2-}) ions compared to other dissolved constituents (Bishop et al., 2014). While extensive research has been conducted on the chemical properties and industrial applications of gypsum, relatively few studies have examined its mechanical behavior under varying stress conditions.

This study seeks to address this gap by investigating the mechanical properties of gypsum through triaxial testing, with a focus on its failure mode, stress-strain response, yield envelope, and Mohr-Coulomb failure criterion. These tests aim to characterize the strength and deformation behavior of gypsum under controlled loading conditions. Additionally, the influence of pore water saturation on mechanical performance will be assessed by preparing gypsum specimens with water contents of 10%, 20%, and 40%. Each sample will be subjected to triaxial loading to evaluate the impact of water content on strength and deformation characteristics.

Other than the mechanical testing, microstructural changes in water-saturated gypsum samples will be examined using X-ray micro-computed tomography (Micro-CT). This technique

will facilitate the visualization and quantification of particle size distribution and structural modifications induced by water absorption. By integrating mechanical and microstructural analyses, this study aims to enhance the understanding of gypsum's mechanical response under different environmental conditions.

2. Method

2.1 Materials

The gypsum used in this study was sourced from Nevada. The sample exhibited an average density of 1.54 g/cm³. Each cylindrical specimen had an average mass of 0.83 g, with an average diameter of 71.5 mm and a height of 149 mm.

2.1.1 Specific Gravity

The specific gravity of the gypsum was determined to be 3.15 through the specific gravity test. The procedure began by filling a 500-ml volumetric flask with de-aired water up to the calibration mark, then the mass of the flask with water and the initial temperature was recorded. Approximately 73 g of air-dried gypsum was measured based on ASTM D-854. The air-dried gypsum was weighed and transferred into a separate 500-ml volumetric flask, then filled with de-aired water to about two-thirds of its capacity.

To eliminate entrapped air, the gypsum-water mixture was heated by boiling the flask for 15–20 minutes while continuously agitating the contents. Proper heating was important to ensure complete air removal, as illustrated in Figure 1. Following this step, the flask was cooled to the initial recorded temperature, and de-aired water was added to bring the volume back to the 500-ml mark. The mixture was then transferred to an evaporative dish and dried in an oven until achieved

constant mass. Finally, the dry gypsum mass was recorded and used to calculate the specific gravity of the material. The specific gravity of the gypsum is calculated:

$$G_s = \frac{M_s}{M_w}$$

where G_s denotes the specific gravity, M_s (g) denotes the mass of soil and M_w (g) denotes the mass of equal volume of water.

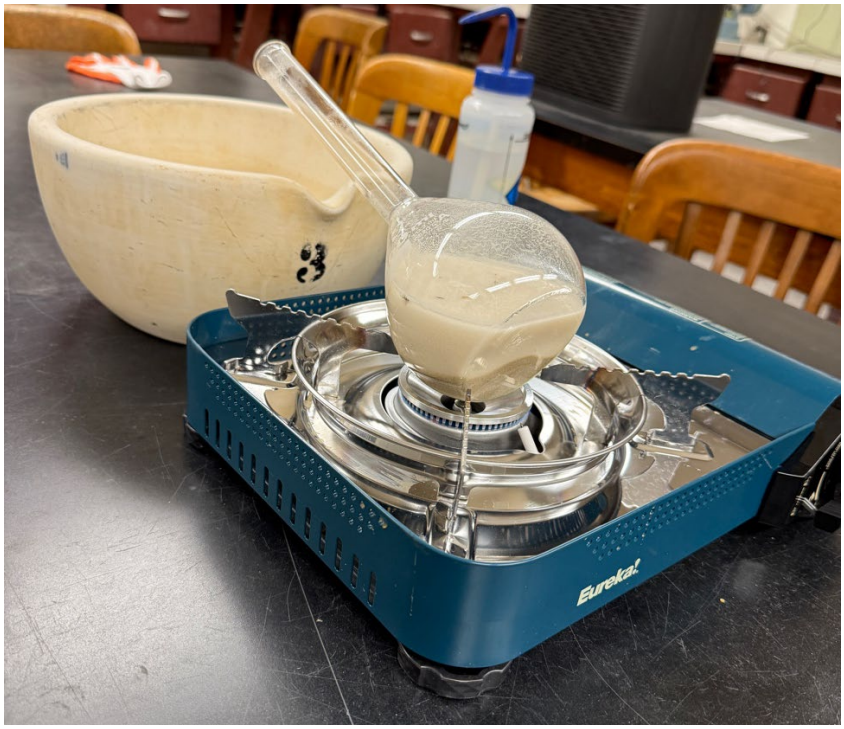

Figure 1: Heating Process to Remove Entrapped Air

2.1.2 Sieve Size

In this study, the grain size distribution of gypsum was determined using sieve analysis. A total of 10 sieves were selected for the test: No. 30, 35, 40, 50, 60, 80, 100, 120, 140, 200, and 400. The largest sieve used was No. 30 with a 0.6 mm sieve opening, while the smallest was No. 400 with a 0.038 mm sieve opening. Each empty sieve was weighed, and its mass was recorded prior to testing. The sieves were then stacked in descending order, with the smallest sieve (No. 400) at the bottom and the largest (No. 30) at the top. A solid-bottom pan was placed beneath the stack to collect finer particles passing through the smallest sieve. Approximately 520 g of gypsum was

poured onto the top sieve, and the stack was placed on a mechanical sieve shaker. The shaking process was conducted for 15 minutes to ensure proper particle separation. As illustrated in Figure 2, half of the sieves were putted on the shakers first that facilitated uniform agitation of the sample. After the test, the sieves were carefully removed from the shaker, and each sieve containing retained gypsum was weighed again. The mass of gypsum retained on each sieve was recorded and used to construct the grain size distribution curve. The results of the sieve analysis are presented in Figure 3.

Figure 2: Half Stack of Sieves in a Sieve Shaker

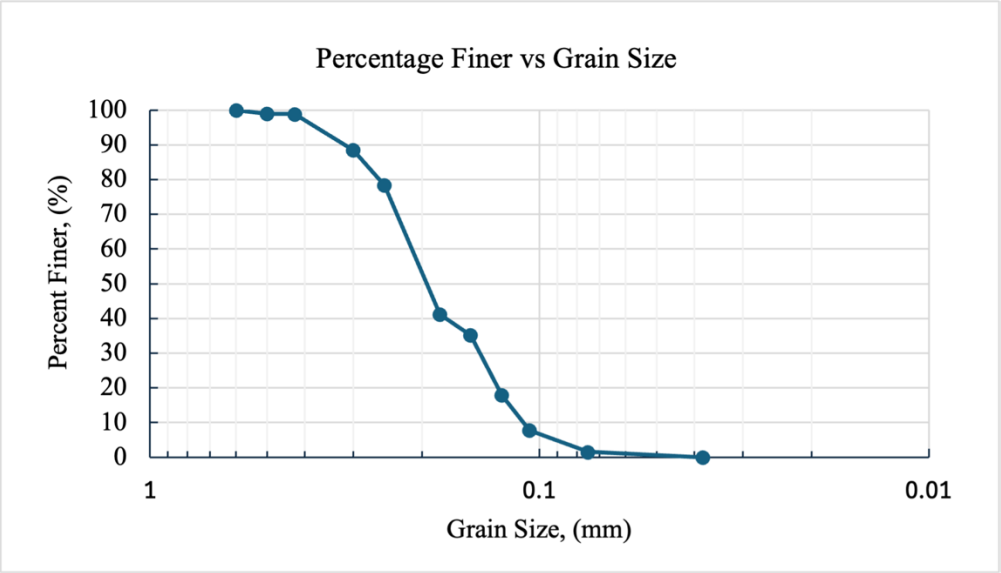

Figure 3: Plot of Percent Finer vs Grain-size
The grain-size distribution obtained from the sieve analysis is plotted with the grain size on a log scale and percent finer on a natural scale.

2.2 Experiment Apparatus

The preparation of the gypsum samples required various tools to ensure a consistent shape and volume. A rubber membrane was used to encase the specimen, maintaining its cylindrical shape throughout the experiment. Porous stones were placed at both the top and bottom of the sample to allow drainage during the test. To prevent air leakage, four elastic rubber rings were secured around the membrane, two at the top and two at the bottom. A two-part vacuum split former (mold) was employed to define the sample volume and shape, while a cylindrical press was used to compact the material and achieve uniform density. The tools used in specimen preparation is illustrated in Figure 4. More details about sample preparation are explained in section 2.3.

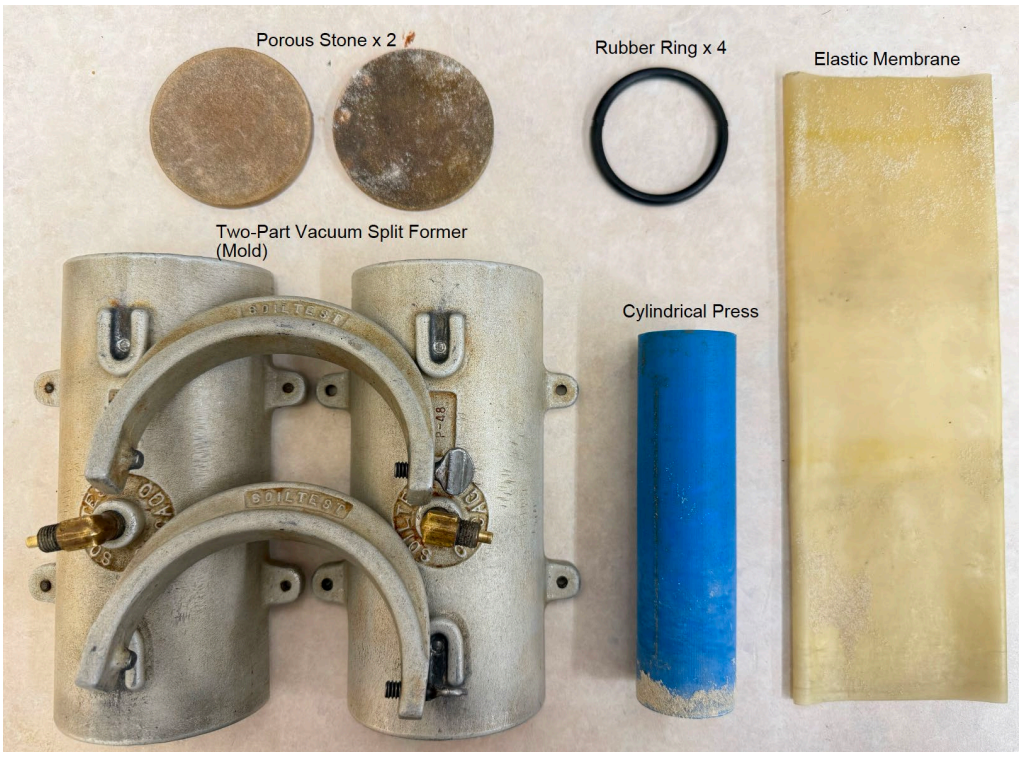

Figure 4: Experiment Apparatus for Sample Preparation
Photograph of the apparatus used during the triaxial test sample preparation.

2.3 Testing Procedure and Sample Preparation

Triaxial testing was conducted using Humboldt triaxial testing equipment to evaluate the mechanical response of gypsum under varying confining pressures and humidity conditions. Two distinct experimental series were performed. The first series focused on dry gypsum specimens subjected to confining pressures of 0.276, 0.414, 0.552, 0.689, and 0.827 MPa to obtain stress-strain relationships and define the material's yield envelope. The second series examined the influence of moisture content on gypsum behavior by testing specimens with water contents of 10%, 20%, and 40% under a constant confining pressure of 0.414 MPa (60 psi).

Sample preparation followed a standardized procedure to ensure consistency across tests. Each gypsum specimen was enclosed within a latex membrane to maintain the volume during loading. The sample preparation started with the placement of a porous stone at the base plate. A latex membrane was then positioned over the porous stone and secured using two elastic rubber

rings to prevent displacement. A two-part vacuum split former was placed around the membrane, serving as a mold to define the sample volume. The upper section of the membrane was folded over the former, then gypsum was placed into the membrane incrementally in successive layers, with each layer compacted using a cylindrical press to ensure uniform density. This process was repeated until the specimen reached approximately 2 cm below the upper boundary of the mold. A second porous stone was then placed atop the gypsum, followed by the triaxial top cap. The membrane was unfolded and secured around the top cap using two additional rubber rings to ensure a tight seal. The vacuum tubes attached to the split former were then removed. The air within the membrane was evacuated using a pressure pump. This was achieved by sequentially opening the valve labeled "top" on the base plate, followed by the three "soft tube" valves on the pressure control panel. The evacuation process continued until no residual air remained, and two tubes were inserted through the top cap was sealed to prevent air leakage. Next, the plexiglass triaxial cell was mounted onto the base plate, with the three lateral rods of the cover securely fastened to the base plate. The cell was filled with water, positioned on the loading machine, and pressurized using the Humboldt pressure panel. For specimens containing added moisture, a predefined volume of water was introduced to achieve target pore saturation levels of 10%, 20%, and 40%. The water was thoroughly mixed with gypsum to ensure homogeneity before specimen compaction. The other steps maintained the same procedure as the sample preparation for the dry gypsum.

All triaxial tests were performed using a Humboldt pressure controller with a maximum load capacity of 50 kN. Axial load measurements were obtained via an S-type load cell (Humboldt HM-2300·100), and a uniform loading rate of 0.8 mm/min was maintained throughout testing. During the loading phase, stress was continuously recorded at 20-second intervals. The test was manually terminated upon reaching shear deformation. The testing equipment used are shown in Figure 5.

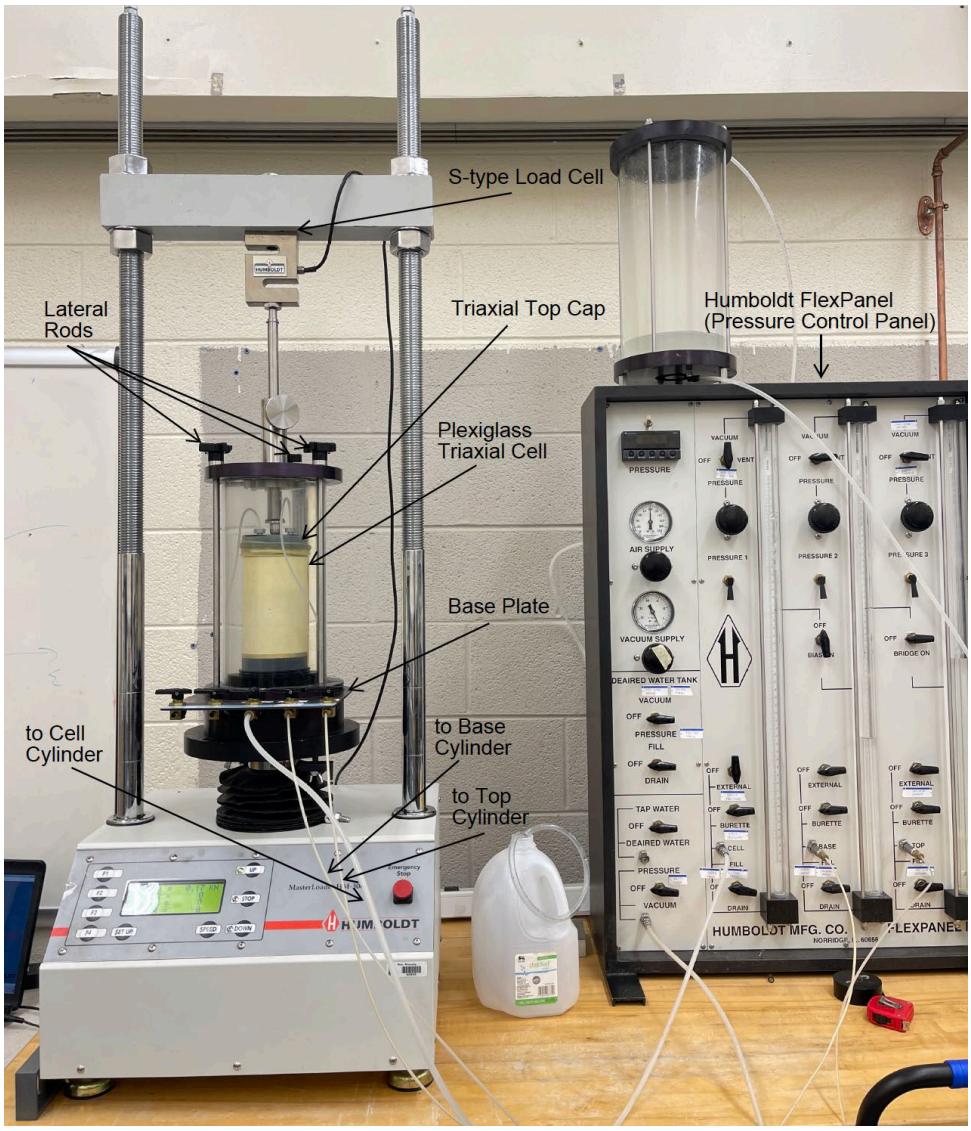

Figure 5: Testing Equipment Used
Photograph of the Humboldt triaxial testing equipment for gypsum. Water is injected through the cell cylinder tube.

2.4 X-Ray Computer Tomography

The TESCAN UniTOM XL X-ray Micro-CT Scanner was employed to examine the internal microstructure of dense materials. In this study, four samples were scanned: (1) original dry gypsum, and (2) a gypsum sample with 10%, 20% and 40% humidity without compression. These scans were conducted to investigate the bonding structures within the samples. High-resolution images obtained from the scans were analyzed using ImageJ software to study

cementation and hydration processes inside the samples. It is also an effective tool for observing grain size evolution with the hydration process. Figure 6 shown the dry gypsum sample placed in the TESCAN CT machine and ready to be scanned.

Figure 6: Dry Gypsum Sample in the TESCAN CT Machine

3. Dry Gypsum Test Results

3.1 Mechanical Failure

The triaxial tests conducted in this study showed the characterization of the stress-strain response of the gypsum samples under varying confinement conditions. To ensure the accuracy and reproducibility of the results, two tests were performed for each of the five confining pressures. The sample underwent plastic deformation, characterized by the occurrence of shear deformation. Shear deformation was observed in all tested samples. As shown in Figure 7, shear bands formed as localized zones of intense strain. Within these bands, grains rearranged and slid past each other under applied stress. Rather than uniform deformation across the sample, movement concentrated in narrow regions. This created distinct boundaries between mobile and stable grains.

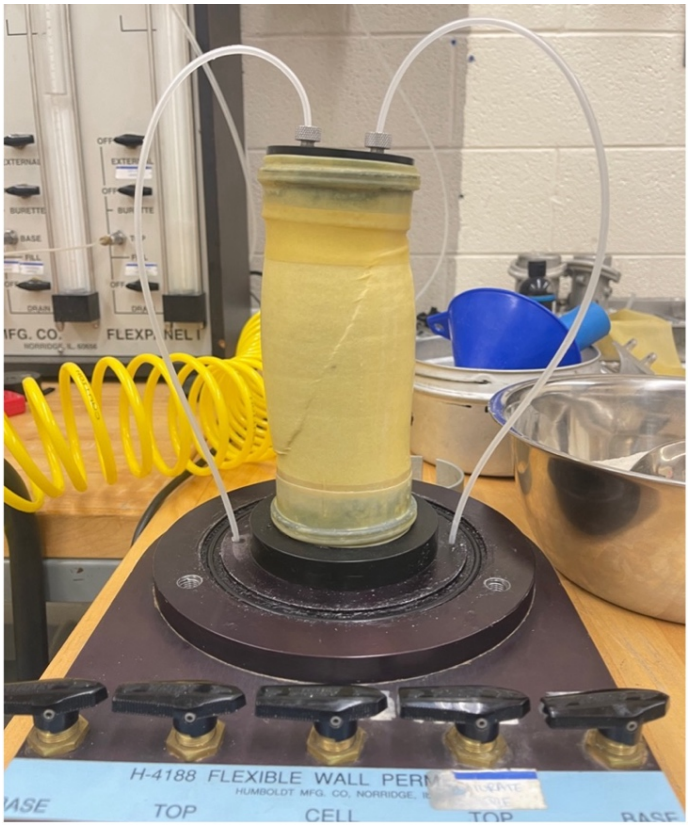

Figure 7 : Shear Deformation of the Dry Gypsum Sample

3.1.1 Stress-Strain Curve

Figure 8 shows the stress-strain curve obtained from the triaxial tests, the tests were carried out with increasing confining stresses of 0.276, 0.414, 0.522, 0.689, and 0.827 MPa. The stress value is calculated using the following equation:

$$\sigma = \frac{F}{A}$$

where σ (MPa) represents the stress, F (kN) denotes the force applied and A (mm^2) denotes the cross-sectional area of the cylindrical gypsum sample. Strain is also calculated by using the following equation:

$$\varepsilon = \frac{L - L_0}{L_0}$$

where ε (mm/mm) is the calculated strain, L is the length after compression measured every 20 seconds, and L_0 is the original length of the gypsum sample.

The stress-strain curves are divided into two regions. The initial region is elastic, after reaching a peak stress, the stress drops, and the sample reaches the plastic domain. The results indicated that the gypsum samples tested within the membrane exhibited ductile behavior, with yielding preceding failure. As illustrated in Figure 8, an increase in confining stress resulted in higher peak stress and strain values, demonstrating that the material can sustain greater deformation before failure. Test 5 conducted under the highest confining pressure of 0.827 MPa, recorded the maximum ultimate stress of 3.61 MPa. The observed trend suggests that with increasing confining pressure, the material exhibits enhanced strength and ductility, leading to a higher stress-strain response. This behavior aligned with the predictions of the Mohr-Coulomb failure criterion.

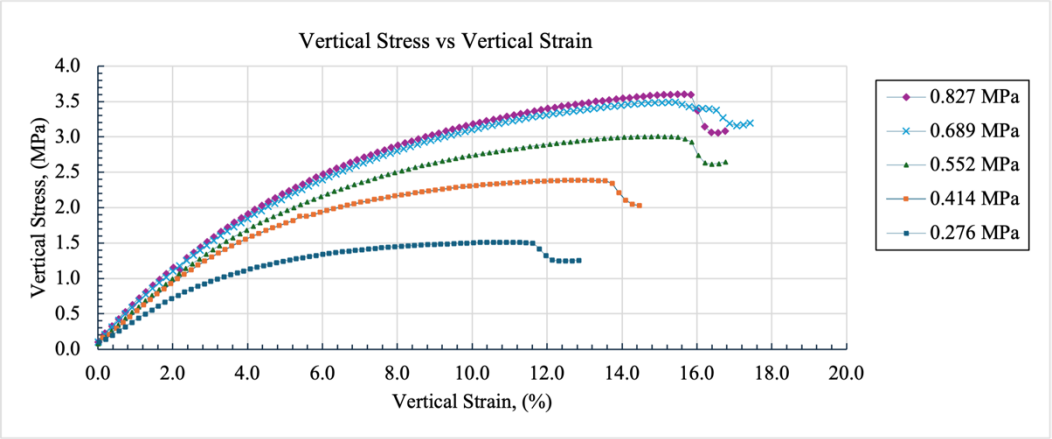

Figure 8: Vertical Stress vs Vertical Strain for the First Round of Tests

3.1.2 Mohr-Coulomb Failure Envelope

The Mohr-Coulomb failure envelope was calculated, providing insight into the material's shear strength as a function of normal stress. As shown in Figure 9, the Mohr circles corresponding to the five triaxial tests were plotted, and the failure envelope was derived accordingly. From this envelope, the cohesion c was determined to be 0.108 MPa, while the internal friction angle ϕ was calculated to be 39°. As confining pressure increased, the material endured higher deviatoric stress, causing the Mohr circles to shift rightward and expand. The black failure envelope represented the shear strength limit, failure will occur when the stress state exceeds this boundary. Additionally, the progressive increase in the radius of the Mohr circles with higher mean effective stress indicated that the material experiences strengthening under elevated confining pressure.

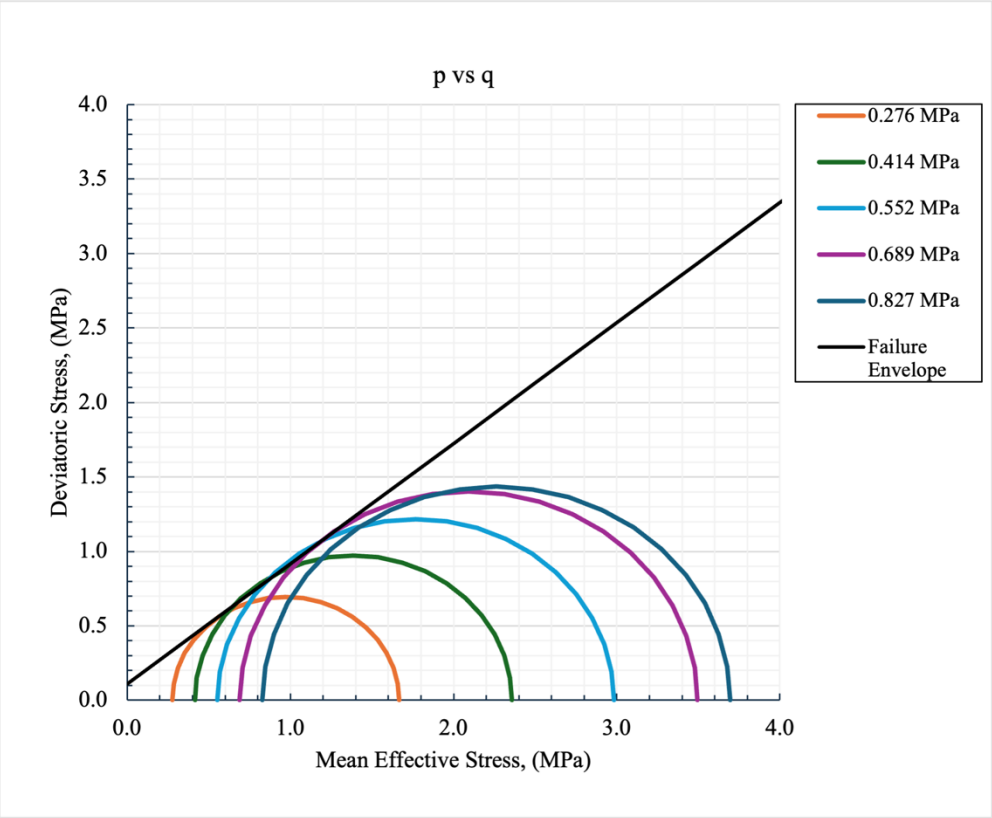

Figure 9: Mean Effective Stress vs Deviatoric Stress

4. Wet Gypsum Test Results

4.1 Mechanical Failure of Wet Gypsum

The mechanical response of gypsum was further investigated by varying its water content, given that gypsum is a water-soluble material which the strength is influenced by pore saturation. In the wet gypsum tests, specimens with pore saturation of 10%, 20%, and 40% were examined under a confining pressure of 0.414 MPa (60 psi). To ensure the reproducibility of the results, each test was performed twice. Figure 10 shows a wet gypsum sample with 40% of pore saturation after the triaxial test. As shown in the picture, the sample exhibited similar deformation behavior as the dry gypsum.

Figure 10: Shear Deformation of the Wet Gypsum Sample (40 %)

4.1.1 Stress-Strain Curve

The stress-strain curves obtained from the triaxial experiments exhibit close alignment due to the consistent confining pressure applied, with comparable peak stresses and similar failure modes observed across all tests. The stress-strain curves are shown in Figure 10.

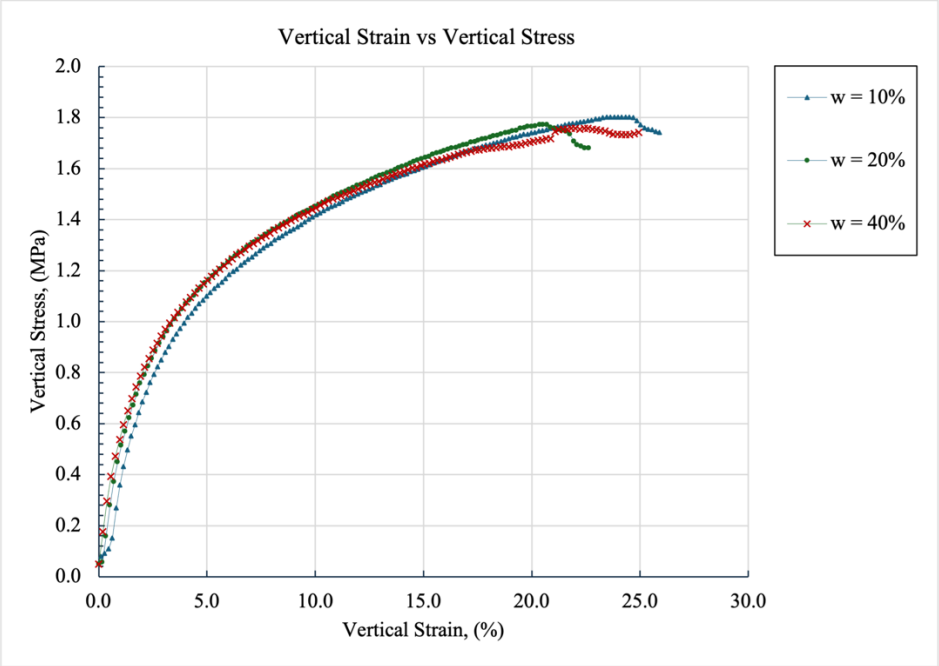

Figure 11: Vertical Stress vs Strain of Wet Gypsum

The stress-strain response of wet gypsum displayed a more distinct phases between the elastic and plastic deformation phases. While the initial stiffness of the wet gypsum samples was comparable to that of the dry gypsum, the post-yield behavior differed significantly. Following the yielding point, wet gypsum exhibited a gradual increase in stress, with a delayed onset of failure. The maximum stress recorded for wet gypsum was 1.8 MPa, whereas the dry gypsum, tested under the same confining pressure of 0.414 MPa, reached a peak stress of 2.38 MPa. This indicates that increased water content within the pore space reduces the material's strength under triaxial loading conditions.

4.1.2 Wet and Dry Comparison Stress-Strain Graph

A comparison between dry and wet gypsum further highlights differences in deformation characteristics. The dry gypsum samples exhibited brittle failure, characterized by a sudden drop in stress upon reaching peak strength. In contrast, wet gypsum demonstrated a more ductile response, as stress continued to increase gradually after yielding, and failure occurred progressively rather than abruptly. The comparison graphs of the dry gypsum and the wet gypsum at 0.414 MPa is shown in Figure 12.

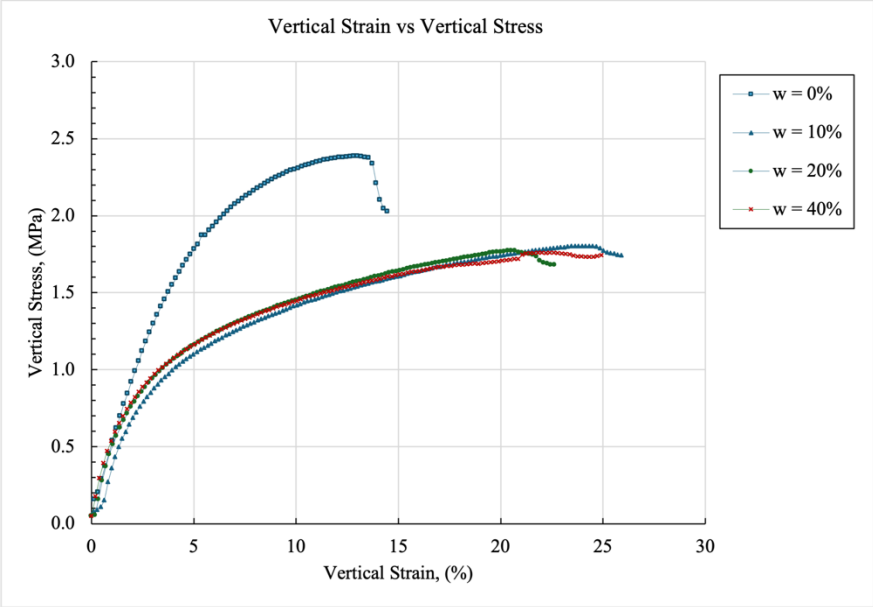

Figure 12: Comparison Graph of Dry Gypsum and Wet Gypsum at 0.414 MPa

The introduction of water into the gypsum matrix led to strain-weakening behavior, suggesting a decrease in the material's resistance to deformation with continued loading. Although the presence of water induced chemical bonding, overall strength of the material was decreased. With water content, the internal structure of the gypsum underwent hydration, potentially involving interlocking of the crystalline framework or alignment of mineral particles. This strain-weakening effect contributed to decrease stress resistance, influencing the mechanical stability of the material under triaxial loading.

5. X-Ray Computer Tomography Results

5.1 Dry Gypsum Scanning Results

Dry gypsum was scanned at 5 μm to examine the internal structure of the dry gypsum sample. The CT-scanned images were reconstructed automatically through TESCAN app, and analyzed using ImageJ, an image processing software. The image presented in Figure 13, is a slice of CT scanned dry gypsum specimen image. In this image, white and gray regions (higher density) correspond to gypsum particles, while black areas (lower density) indicate the presence of air voids or pores within the sample. The gypsum particles exhibited a range of sizes and shapes, with some appearing elongated and others more circular in form.

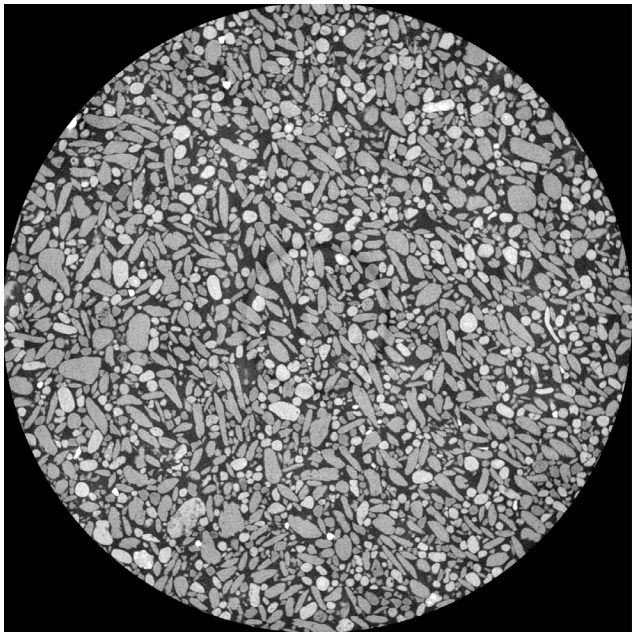

Figure 13: A Slice of CT Scanned Dry Gypsum Image

5.2 Compressed Sample vs. Non-Compressed Sample Scanning Results

The scanning results from the 40% moisture content samples, both with and without compression revealed key insights into gypsum's bonding characteristics as shown in Figure 14. Figure 14(a) represented the uncompressed sample, which was preprepared and allowed to set overnight before CT scan. This was done to determine the observed cementation resulted from

capillary bonding due to compression or was purely a product of chemical bonding. The results indicated that even without compression, gypsum observed cementation, suggesting that chemical bonding occurred due to change of water content is purely chemical. Figure 14(b) represented a gypsum sample that was scanned right after the triaxial test. In this slice of image, the presence of darker cracks suggested the failure points formed within the structure. These fractures indicated area where stress was concentrated, leading to localized mechanical weakness.

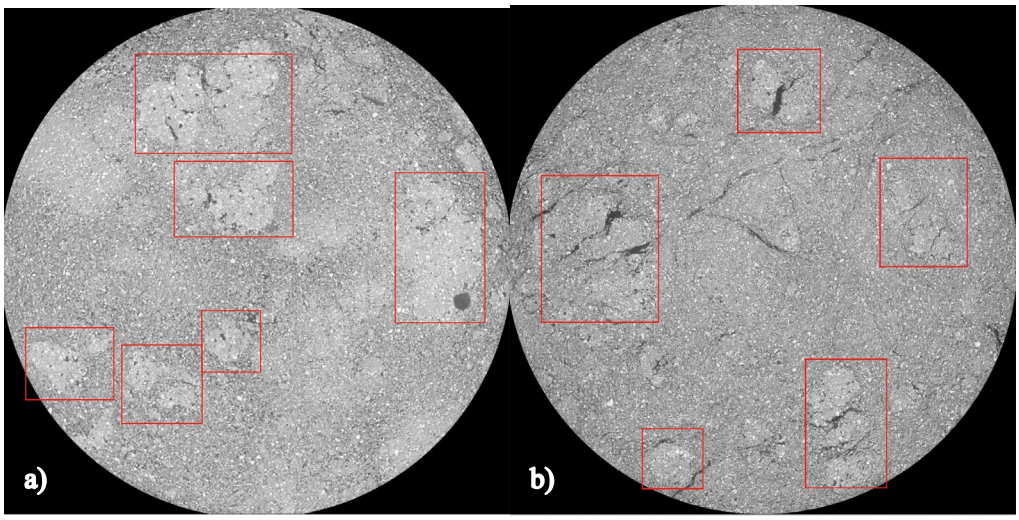

Figure 14: Comparison Pictures of Scanned 40% Moisture Gypsum Sample (a) and Scanned Wet Gypsum with Applied Compression. Both samples showed cementation.

5.3 Wet Gypsum Scanning Results

For microstructure findings, the 10% and 20% moisture content sample were scanned at a resolution of 46 microns, while the 40% moisture content sample was scanned at a finer resolution of 15 microns. The CT scanned images of the wet gypsum samples showed varying degrees of chemical bonding with different moisture percentage. Three representative images were selected from each stack of scanned images to illustrate the trends.

For the gypsum sample with 10% water content as shown in Figure 15, minimal cementation was observed, indicating limited particle interactions. As the water content increased to 20%, larger regions of cementation was found as shown in Figure 16, suggesting that moisture

facilitated bond formation between gypsum particles. At 40% water content, the area of cementation within the sample was significantly increased. As shown in Figure 17, the white or light gray areas. The observed scanned images suggest a trend: higher moisture levels promote stronger particle interactions and the bond formation.

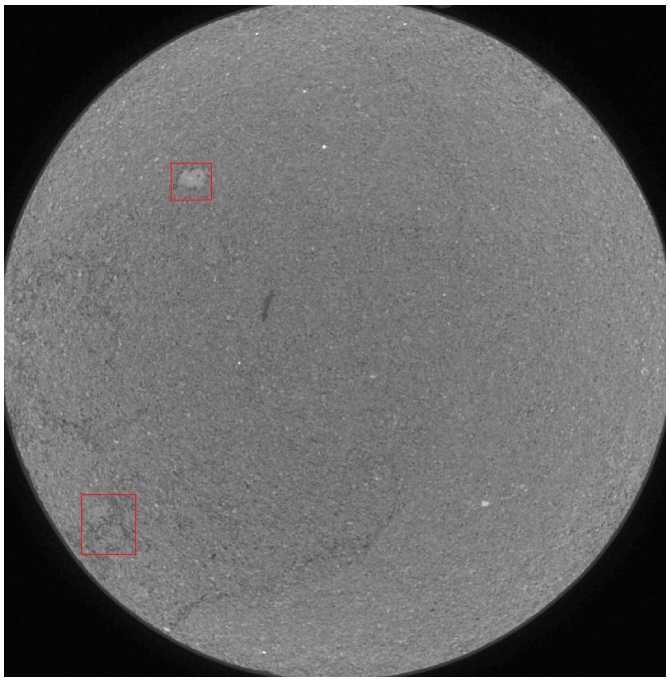

Figure 15: Scanned Image of Gypsum Sample with 10% Moisture Content

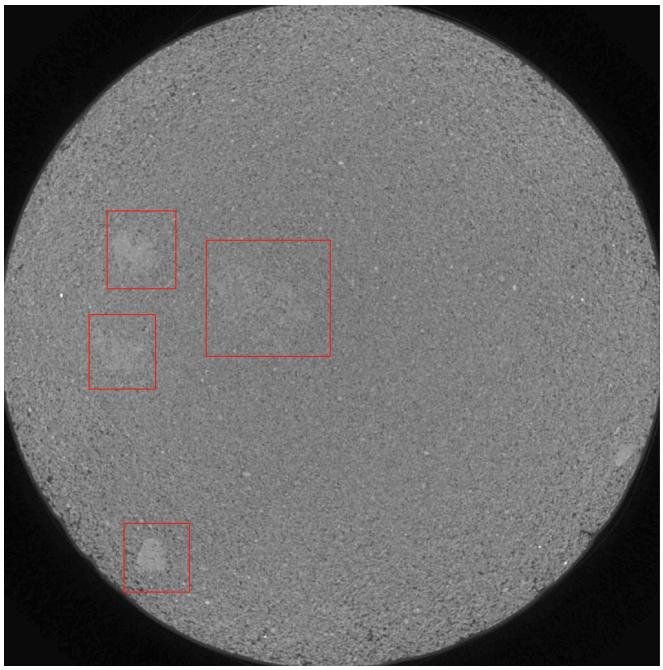

Figure 16: Scanned Image of Gypsum Sample with 20% Moisture Content

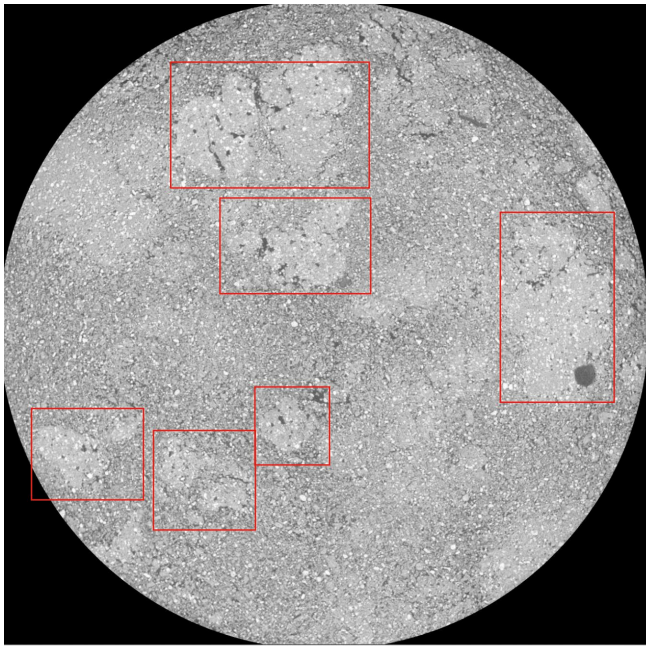

Figure 17: Scanned Image of Gypsum Sample with 40% Moisture Content

6. Conclusion

This study examined the mechanical properties of gypsum through triaxial testing and X-ray micro-computed tomography (Micro-CT) analysis, providing insights into its strength, deformation behavior, and microstructural characteristics under varying confining pressures and moisture conditions. The experimental results demonstrated that dry gypsum exhibits a ductile failure mode, with increasing confining pressure resulting in higher strength values. The failure envelope analysis confirmed the applicability of the Mohr-Coulomb failure criterion, with cohesion and internal friction angle determined accordingly.

The effect of percentage of pore saturation on gypsum's mechanical response was also investigated, revealing that increasing water content reduces peak strength with increasing yielding time before plastic deformation. Wet gypsum exhibited strain-weakening behavior, suggesting that the presence of water facilitates particle cementing, thereby influencing the material's stress-strain response. A decrease in maximum recorded stress with increasing pore saturation further confirmed the adverse impact of moisture on gypsum's load-bearing capacity.

Micro-CT analysis provided a detailed assessment of the internal structure, particle distribution, and bonding within the samples. The scanning results from the compressed and uncompressed wet gypsum indicated that bonding within sample is purely chemical and water induced in the gypsum samples occurred cementation. Moisture content influenced degrees of cementation, with increasing moisture content (10%, 20%, and 40%) the regions of bonding was also increased as shown in the scanned images. These findings contribute to a better understanding of gypsum's behavior under different environmental conditions.

Future research could incorporate in situ Micro-CT scanning during saturation of the gypsum sample to observe real-time microstructural evolution. Additionally, coupling this approach with pressure solution experiments would offer more insights into grain contact evolution,

dissolution-precipitation mechanisms, and their influence on the deformation and strength characteristics of gypsum.

References

Bishop, J. L., Lane, M. D., Dyar, M. D., King, S. J., Brown, A. J., & Swayze, G. A. (2014). Spectral properties of ca-sulfates: Gypsum, Bassanite, and anhydrite. *American Mineralogist*, *99*(10), 2105–2115. https://doi.org/10.2138/am-2014-4756

del Río-Merino, M., Vidales-Barriguete, A., Piña-Ramírez, C., Vitiello, V., Santa Cruz-Astorqui, J., & Castelluccio, R. (2022). A review of the research about gypsum mortars with waste aggregates. *Journal of Building Engineering*, *45*, 103338. https://doi.org/10.1016/j.jobe.2021.103338

Garg, M., & Pundir, A. (2014). Investigation of properties of fluorogypsum-slag composite binders – hydration, strength and microstructure. *Cement and Concrete Composites*, *45*, 227–233. https://doi.org/10.1016/j.cemconcomp.2013.10.010

Jin, Q., Perry, L. N., & Bullard, J. W. (2020). Temperature dependence of gypsum dissolution rates. *Cement and Concrete Research*, *129*, 105969. https://doi.org/10.1016/j.cemconres.2019.105969